HHS Public Access

Author manuscript

Exp Neurol. Author manuscript; available in PMC 2024 May 01.

Published in final edited form as:

Exp Neurol. 2023 May ; 363: 114354. doi:10.1016/j.expneurol.2023.114354.

Impaired neurogenesis with reactive astrocytosis in the hippocampus in a porcine model of acquired hydrocephalus

Maria Garcia-Bonilla[1], **Arjun Nair**[1], **Jason Moore**[1], **Leandro Castaneyra-Ruiz**[2], **Sarah H. Zwick**[1], **Ryan N. Dilger**[3,4], **Stephen A. Fleming**[3,4], **Rebecca K. Golden**[3], **Michael R. Talcott**[1,5], **Albert M. Isaacs**[6], **David D. Limbrick Jr.**[1], **James P. McAllister II**[1]

[1]Department of Neurosurgery, Washington University in St. Louis School of Medicine, St. Louis, Missouri, 63110, USA.

[2]CHOC Children's Research Institute, 1201 W. La Veta Avenue, Orange, CA, 92868, USA.

[3]Neuroscience Program, Department of Animal Sciences, University of Illinois, Urbana-Champaign, Illinois 61801, USA.

[4]Traverse Science, Champaign, IL 61801, USA.

[5]AbbVie, Inc. North Chicago, IL, 60064, USA.

[6]Department of Neurological Surgery, Vanderbilt, University Medical Center, Nashville, Tennessee, 37232, USA.

Abstract

Background: Hydrocephalus is a neurological disease with an incidence of 0.3–0.7 per 1,000 live births in the United States. Ventriculomegaly, periventricular white matter alterations, inflammation, and gliosis are among the neuropathologies associated with this disease. We hypothesized that hippocampus structure and subgranular zone neurogenesis are altered in untreated hydrocephalus and correlate with recognition memory deficits.

Corresponding Author: Maria Garcia-Bonilla, mariag@wustl.edu.

AUTHOR CONTRIBUTIONS

MG-B conceived the study and designed the experimental approach, performed or assisted in animal procedures, performed data collection and analyses, helped maintain animal protocols, and wrote the manuscript. LC-R assisted in all animal procedures, performed some experimental analyses, and edited the manuscript. AN, JM and SHZ assisted in part of the animal procedures and data analyses, and edited the manuscript.

RND, RKG, and SAF designed the cognitive testing experiments, analyzed data, and edited the manuscript. MT performed or assisted in all animal procedures, edited animal protocols and edited the manuscript. DMM provided advice on the experimental design, assisted in data analyses, and edited the manuscript. DDL conceived the study, obtained funding, performed or assisted in all surgical treatment procedures, assisted data collection and analyses, and edited the manuscript. JPM helped conceive and directed the study, obtained funding, performed or assisted in all animal procedures, assisted data collection and analyses, and wrote and maintained animal protocols. All authors read and approved the final manuscript.

Competing interests

No competing interests to declare.

Ethics approval and consent to participate

No human subjects or tissue

Availability of data and materials

All data generated or analyzed during this study are included in this published article and its additional information files.

Methods: Hydrocephalus was induced by intracisternal kaolin injections in domestic juvenile pigs (43.6 ± 9.8 days). Age-matched sham controls received similar saline injections. MRI was performed to measure ventricular volume, and/or hippocampal and perirhinal sizes at 14 ± 4 days and 36 ± 8 days post-induction. Recognition memory was assessed one week before and after kaolin induction. Histology and immunohistochemistry in the hippocampus were performed at sacrifice.

Results: The hippocampal width and the perirhinal cortex thickness were decreased ($p<0.05$) in hydrocephalic pigs 14 ± 4 days post-induction. At sacrifice (36 ± 8 days post-induction), significant expansion of the cerebral ventricles was detected ($p=0.005$) in hydrocephalic pigs compared with sham controls. The area of the dorsal hippocampus exhibited a reduction ($p=0.035$) of 23.4 % in the hydrocephalic pigs at sacrifice. Likewise, in hydrocephalic pigs, the percentages of neuronal precursor cells (doublecortin+ cells) and neurons decreased ($p<0.01$) by 32.35 %, and 19.74 %, respectively, in the subgranular zone of the dorsal hippocampus. The percentage of reactive astrocytes (vimentin+) was increased ($p=0.041$) by 48.7 %. In contrast, microglial cells were found to decrease ($p=0.014$) by 55.74 % in the dorsal hippocampus in hydrocephalic pigs. There was no difference in the recognition index, a summative measure of learning and memory, one week before and after the induction of hydrocephalus.

Conclusion: In untreated juvenile pigs, acquired hydrocephalus caused morphological alterations, reduced neurogenesis, and reactive astrocytosis in the hippocampus and perirhinal cortex.

Keywords

acquired hydrocephalus; pig model; hippocampus; perirhinal cortex; recognition memory; neurogenesis; neuroinflammation

INTRODUCTION

Hydrocephalus is the most common neurological disorder treated by pediatric neurosurgeons (Kahle et al., 2016) with an incidence of 0.3–0.7 per 1,000 live births in the United States (Isaacs et al., 2018). It is a disease resulting from an imbalance in cerebrospinal fluid (CSF) production and absorption, producing an expansion of the brain ventricles with increases in intracranial pressure (Rekate, 2011; Tully and Dobyns, 2014; Kahle et al., 2016; Garcia-Bonilla et al., 2021). Despite improvements in treatment, neurological deficits are frequent and include cognitive and sensorimotor impairments (Erickson et al., 2001; Robinson, 2012; Zielińska et al., 2017).

The neuropathology of hydrocephalus is multifactorial and includes ventriculomegaly, ischemia/hypoxia, ventricular/subventricular zone disruption (Domínguez-Pinos et al., 2005; Jiménez et al., 2009; McAllister, 2012; Guerra et al., 2015; Garcia-Bonilla et al., 2022), and periventricular white matter cytopathology (Del Bigio et al., 2003; Del Bigio, 2010; McAllister, 2012; Goulding et al., 2020). Experimental and clinical studies have shown that inflammation also plays a role in the pathogenesis of acquired hydrocephalus (Karimy et al., 2020) through enhanced reactivity of microglial and astroglial cells (Shirane et al., 1992; da Silva, 2005; McAllister, 2012; Furey, 2019), as well as increased levels of pro-inflammatory

cytokines and chemokines, such as interleukins IL1, IL6, tumor necrosis factor-alpha (TNF alpha), or transforming growth factor-beta, in the CSF (Mangano et al., 1998; Gram et al., 2013; Jiménez et al., 2014; Chaudhry et al., 2017; Czubowicz et al., 2017; Habiyaremye et al., 2017; Sharma et al., 2017; Olopade et al., 2019; Goulding et al., 2020; Karimy et al., 2020; Garcia-Bonilla et al., 2022).

Pertinent to the learning disabilities and hippocampal impairments associated with hydrocephalus (Garton et al., 2016; Strahle et al., 2019; Paturu et al., 2022), rodent and feline models of pediatric hydrocephalus have demonstrated increased cell death and loss of dendritic arbors in the hippocampus, and learning and memory deficits (Kriebel and McAllister, 2000; Chen et al., 2017; Turgut et al., 2018; Femi-Akinlosotu et al., 2021). However, hippocampal alterations and their relationship with ventricular volume and recognition memory in larger animal models of hydrocephalus are still unexplored. Recognition memory denotes the ability to distinguish familiar from novel objects and places (Wang et al., 2021). Although the role of the hippocampus in recognition memory has been debated (Barker and Warburton, 2011), lesion studies have demonstrated that recognition memory involves a large network that includes the hippocampus and the perirhinal cortex (Warburton and Brown, 2010; Wang et al., 2021). In rodents and pigs, the hippocampus has been classically divided into two major parts: dorsal (anterior in humans) and ventral (posterior in humans), each of which receives different connections from cortical and subcortical areas (Voss et al., 2017; Tzakis and Holahan, 2019). Furthermore, the hippocampus contains the subgranular zone (SGZ): the neurogenic niche in which new neurons can be generated from neuronal progenitor cells (doublecortin – DCX positive cells) (Kempermann et al., 2015; Fares et al., 2019), which can be relevant for learning and memory tasks (Lee and Son, 2009; Lieberwirth et al., 2016; Alam et al., 2018).

Our group has successfully developed a large animal model of acquired hydrocephalus (McAllister et al., 2021; Garcia-Bonilla et al., 2022) by injecting kaolin (aluminum silicate) into the cisterna magna using methods similar to those in other species (Eskandari et al., 2004; Li et al., 2008; Lopes Lda et al., 2009; Eskandari et al., 2011; Di Curzio et al., 2013; Jusué-Torres et al., 2016; Curzio, 2018). Obstructing CSF flow occurs as a result of a local inflammatory reaction and fibrous scarring (Khan and Del Bigio, 2006; Lopes Lda et al., 2009; Curzio, 2018). This pig (*Sus scrofa domesticus*) model facilitates studies of human brain diseases due to several anatomical and physiological similarities to humans (Lind et al., 2007; Conrad et al., 2012; Wixey et al., 2019), and the relatively large brain size enables the performance of the same neurosurgical treatments for patients with hydrocephalus (Kulkarni et al., 2018; Riva-Cambrin et al., 2019; Coulter et al., 2020; Pindrik et al., 2020; McAllister et al., 2021).

The present investigation aimed to study the neuropathology of acquired hydrocephalus in a pig model to test the hypothesis that hippocampal structure and SGZ neurogenesis are altered in untreated hydrocephalus and correlate with recognition memory deficits.

MATERIALS AND METHODS

Animals

Juvenile female pigs (*Sus scrofa domesticus*), with a mean age of 43.6 ± 9.8 days at hydrocephalus or sham induction, were used (Additional Table 1). Females were preferred because they exhibit more exploratory behavior than males (Fleming and Dilger, 2017), and thus were more sensitive to the cognitive assessments (McAllister et al., 2021). Animals were separated into two cohorts (see Additional Table 1 for details):

1. To assess recognition memory and to quantify hippocampal, ventricular, and perirhinal cortex sizes using magnetic resonance imaging (MRI) at 14 ± 4 days post-induction (mean age of 58.9 days, n = 20).
2. To analyze neuropathology at 36 ± 8 days post-induction (mean age of 74.4 days; time determined by the development of hydrocephalus clinical symptoms), hydrocephalus, n = 7; and sham control, n = 6.

Pigs were obtained from Oak Hill Genetics LLC (Ewing, IL, USA) and housed at the Washington University in St. Louis vivarium in standard pens with raised flooring, fed with a nutritionally-adequate, age-appropriate diet (Purina Porcine Grower Diet 5084), and provided access to water ad libitum. Before any procedure, the pigs were acclimated to the facility and personnel for at least 3 days, and their health was confirmed by the institutional veterinary staff. The design of the experiments, housing, handling, care, surgery, and pre/post-operative management of the animals were approved by the Washington University Institutional Animal Care and Use Committee and performed in an AAALAC-accredited facility in compliance with the Guide for the Care and Use of Laboratory Animals and the Animal Welfare Act.

Induction of hydrocephalus

Using sterile technique, an 18-gauge spinal needle was used to access the cisterna magna as previously described (McAllister et al., 2021; Garcia-Bonilla et al., 2022). Briefly, animals were sedated, intubated, and anesthetized with 2.5% isoflurane in O_2. After the collection of 1 ml of CSF to confirm access, 1.3 ml of sterile 25% kaolin (K2502, Aqua Solutions, Deer Park, TX, US) suspension was injected over 5 minutes into the cisterna magna. Sham controls received injections of sterile saline.

Animals were observed post-procedure for signs of fever, pain, and neurological impairment (locomotor or sensorimotor behavior impairment, ataxia, imbalance, loss of alertness) and their ability to eat and drink every 4 h for the next 12–15 h, and daily for the following 10 days. They received subcutaneous injections of buprenorphine (0.12–0.24 mg/kg) or carprofen (2–4 mg/kg) to reduce potential pain, and acetaminophen (162.5 mg) was given rectally to reduce fever if needed in a case-by-case basis.

Magnetic resonance imaging

MRI was performed at 14 ± 4 days post-induction (mean age of 58.9 days), and at sacrifice (36 ± 8 days post-induction, mean age of 74.4 days) (Additional Table 1). Pigs were sedated and anesthetized as described above. Pulse oximetry, respiration, and body temperature were

monitored every 15 minutes during imaging. The images were attained with a Siemens Prisma 3.0-Tesla MR scanner with a 60-cm bore diameter, a 20-channel head coil, an 80 mT/m gradient field, and a slew rate of 200 mT/ms. T1- and T2-weighted images (0.9 mm of slice thickness) were obtained with a 3D fast spin-echo sequence with an echo train length of 8, Field of view 205×205 mm (256×256 voxels), and a voxel size of 0.8 mm^3. T2 and T1 weighted magnetization-prepared rapid acquisition with gradient echo (MPRAGE) scan time varied from 4–11 minutes (T1:Repetition time (TR) 2300 ms, Time to Echo (TE) 2.36 ms, 2 averages; T2:TR 3200 ms, TE 409 ms, 2 averages).

Ventricular and total brain volume, hippocampal and perirhinal cortex size analyses

Analyses of ventricular volumes were calculated from the MRI performed at 14 ± 4 days post-induction (mean age of 58.9 days), and at sacrifice (36 ± 8 days post-induction, mean age of 74.4 days) (Additional Table 1) using the sagittal, axial, and coronal T2 MRI images (0.9 mm) and the software ITK-SNAP v3.8.0 (http://www.itksnap.org/pmwiki/pmwiki.php, University of Pennsylvania, US). The ventricles were manually segmented, and the volume was calculated in mm^3 using the volumes and statistics tools. Ventricular volume was normalized by total brain volume in each animal (i.e., expressed as % of total brain volume). Structures included in the total brain volumes were the olfactory bulbs, cerebral cortex, neostriatum, diencephalon (thalamus and hypothalamus), cerebellum, and the brain stem from the mammillary bodies extending posteriorly to the terminus of the fourth ventricle. Excluded from the total brain volume measurements were the pituitary gland, cranial nerves, the cisterna magna, basal cisterns, quadrigeminal cisterns, as well as CSF from the anterior and posterior longitudinal cerebral fissure. Olfactory, lateral, third, and fourth ventricles were all included in ventricle volume measurements. For the simple linear regression, the size of the different parts of the lateral ventricle close to the hippocampus (the body, from the foramen of Monro to the point where the septum pellucidum ends and the corpus callosum and fornix meet - hippocampal commissure; the atrium, a triangular cavity that opens anteriorly into the body and basely into the temporal horn; and temporal horn, that extends anteriorly from the atrium below the thalamus and terminates at the amygdala) was measured using the methods previously described(Garcia-Bonilla et al., 2022).

The length and width of the total and dorsal hippocampus, and the perirhinal thickness, were measured at 14 ± 4 days post-induction (mean age of 58.9 days), (Additional Table 1) using Horos (LGPL license at Horosproject.org and sponsored by Nimble Co LLC d/b/a Purview in Annapolis, MD, USA). For the entire hippocampus, three serial MRI coronal sections (0.9 mm of slice thickness) from anterior to posterior were analyzed starting at the beginning of the cerebral aqueduct. For the dorsal hippocampus, three serial MRI sagittal sections from the midline to lateral were analyzed starting at the third section laterally from the midline. Matched images were studied for both groups. For the perirhinal cortex thickness, three serial MRI coronal sections (0.9 mm thickness) from anterior to posterior were used starting when the ventral hippocampus ended (that occurred close to the medial part of the cerebral aqueduct). The perirhinal cortex was delimited by the rhinal sulcus laterally and the inferior medial floor of the temporal horn of the lateral ventricle superiorly [following the boundaries described in humans (Bouyeure et al., 2018; Zhernovaia et al., 2020)].

Behavioral and cognitive testing

To quantify cognitive function, pigs were tested prior to and one week following hydrocephalus induction (Additional Table 1). A novel object recognition (NOR) task was used following validated procedures (Dilger and Johnson, 2010; Fleming and Dilger, 2017; Fleming et al., 2019). The paradigm began with two habituation days to allow familiarization to the testing environment. Habituation days were consecutive and allowed pigs to explore an empty arena for 10-min each day. The sample trial was performed on the third day and pigs were allowed 5-min to explore 2 identical objects secured to the floor. After a 48-hour delay period, pigs performed the test trial where they were given 5-min to explore 1 familiar object from the sample trial and 1 novel object. Each trial was recorded with a video camera suspended over the arena. A single, unbiased, trained observer annotated and scored the continuous recordings to calculate the following measurements: (1) number of visits to novel/sample objects, (2) time investigating novel/sample objects, (3) mean length of time per visit to an object, (4) latency to the first object visit, and (5) latency to the last object visit. Raw data output from Loopy (http://loopb.io, loopbio gmbh, Vienna, Austria) was then fed through a Python script to standardize the calculation of all measures before running comparative statistics. The primary outcome for cognition was recognition index (RI), which was calculated per pig as time spent investigating the novel object as a proportion of the total investigation time of both objects during the test trial. RI > 0.50 significantly indicates novelty preference and thus recognition memory (Dilger and Johnson, 2010; Fleming and Dilger, 2017).

Histology and immunofluorescence

Tissue fixation was performed in animals at sacrifice (36 ± 8 days post-induction, mean age of 74.4 days). They were sedated and administered intravenous heparin (150 mg/kg). Pigs were sacrificed under anesthesia with intravenous sodium pentobarbital (120 mg/kg), transcardially perfused with phosphate-buffered saline (PBS, 0.1 M pH 7.2) followed by 4% paraformaldehyde diluted in the same buffer, and postfixed for 48 h at room temperature.

Fixed brains were embedded in paraffin and sectioned serially in the coronal plane at a thickness of 10 μm using standard procedures. After heat-induced antigen retrieval in citrate (50 mM, pH 6.0), primary antibodies (Table 1) were incubated for 18 h at 22 °C. Secondary antibodies conjugated with Alexa Fluor 488 or Alexa Fluor 555 (RRID: AB_2576217, AB_2535844, AB_2534069, Thermo Fisher, Waltham, MA) were applied for 1 h at room temperature, dilution 1:500. 4′,6-Diamidino-2-phenylindole dihydrochloride (DAPI, Molecular probes Life technology, D1306, RRID: AB_2629482) was used for nuclear staining, dilution 1:5000, 5 minutes. The antibodies were diluted in PBS containing 0.1% Triton X-100 (Sigma) and 10% normal serum (Sigma).

Hematoxylin-eosin histochemistry

Hematoxylin (Harris, Biocare Medical, CA, US, 061920A-2) was applied for 5 minutes, rinsed for 5 minutes in running tap water, and differentiated by a fast dip in 0.5% acid ethanol in paraffin sections that were previously deparaffinized and hydrated. Then, sections were stained with 0.5% eosin (Sigma, 1.09844.1000) for 3 minutes, dehydrated, and mounted with xylene-based mounting medium.

Image analysis and quantifications

Immunofluorescent images (1024 × 1024-pixel resolution) were obtained with a Zeiss LSM 880 Airyscan Two-Photon Confocal Microscope (Oberkochen, Germany) and Zeiss Axial Imager Z2 fluorescence microscope with Apotome 2. Bright-field visualization was obtained with a Zeiss Axio Scanner Z1. For each experiment, images were obtained in batches using the same settings. Figures were composed using PowerPoint (Microsoft Office 365, Albuquerque, New Mexico, US) and ZEN 3.4 Blue Edition (Zeiss), and the same minimal changes in brightness and contrast were applied.

The cell densities of neuronal progenitor cells (DCX+), neurons (NeuN+), reactive astrocytes (vimentin+), microglia (ionized calcium-binding adaptor molecule 1 - Iba1+), were calculated in 3 fields of 3 different areas per parietal cortex section per animal. The densities were normalized by the total number of cells (DAPI+ cells) in each picture and expressed as the percentage of cells. The hippocampal area and thickness of the CA1 layers were quantified in 1 every 60 sections (600 μm) in the entire hippocampus of each animal. On average, 3 sections separated by intervals of 600 μm per animal were quantified using ImageJ software. The hippocampus was defined as the area between the CA1-subiculum border and an artificial vertical border drawn at the lateral-most part of the fimbriae fornix. The area of the sections was calculated by outlining the perimeter of the tissue between these borders and normalized by total brain volume. To normalize, each area was divided by total brain volume (see MRI paragraph for a detailed explanation of total brain volume measurement) in each case. The thickness of the seven CA1 layers was measured in all sections as the percentage of the total CA1 thickness: Alveus (A), Stratum Oriens (O), Stratum Pyramidale (P), Stratum Radiatum (R), Stratum Lacunosum-Moleculare (L-M), Stratum Moleculare (M), and Stratum Granulosum (G). Finally, the percent change in ventricular volumes was calculated as the increase between the ventricular volume mean of the sham controls and ventricular volumes of each hydrocephalic pig divided by the sham mean and multiplied by 100. The percent change in RI was calculated as the change between RI pre- and post-induction of hydrocephalus in each hydrocephalic pig divided by the pre-induction value and multiplied by 100.

Statistical analysis

Statistical analyses were performed using GraphPad Software (San Diego, CA, USA) and SAS (Raleigh, NC, US). Animals were numbered without indication of the group. All values are reported in the figures as mean ± standard deviation (SD). Mann-Whitney test and Student's t-test were applied for hypothesis testing in situations requiring non-parametric and parametric analyses, respectively (shown with * in the graphs in the figures). Normality was previously analyzed by normality and lognormality tests (Anderson-Darling test, D'Agostino-Pearson omnibus normality test, Shapiro-Wilk normality test, and Kolmogorov-Smirnov normality test with Dallal-Wilkinson-Lillie for p-value). Simple linear regression analysis was performed to model the relationship between the hippocampus area and ventricular volume, vimentin+, iba1+, DCX+, and NeuN+ cells; and % change in RI versus % change in ventricular volume and hippocampal size. When the F probability from Student's t-test was < 0.05, the variance was considered unequal. $P < 0.05$ based on both tests was considered statistically significant.

Interpretation of NOR data was focused on the primary NOR outcome, RI, which is the proportion of time spent exploring the novel object compared to the total exploration time of both objects. The statistical approach involved a one-tailed t-test to compare the recognition index with a chance performance value of 0.50 (i.e., exploration of one object over the other for 50% of the total exploration time). A RI of 0.50 was considered chance exploration due to the task comparing data of two objects (one familiar object and one novel object). As mentioned above, a RI greater than 0.50 was interpreted as a subject displaying novelty preference, and thus recognition memory. The number of visits per object, time spent per object, and latency to the first or last object were compared using a one-way ANOVA which included a single fixed effect of time-point.

RESULTS

Ventricular volume in the pig model of hydrocephalus

MRI examinations at sacrifice showed the dilatation of all portions of the cerebral ventricles (Fig. 1A, Supplemental Fig. 1). The mean proportion of ventricular volume, expressed as a percentage of total brain volume, in sham control pigs was 3 ± 0.4 %, while hydrocephalic pigs exhibited ventricular dilation with a mean of 11.1 ± 8.2 % (p=0.001, Mann-Whitney test) (Fig. 1B).

Hippocampal area and thickness of the hippocampal layers

The hippocampal area and the thickness of the hippocampal layers in the CA1 were analyzed in sham control and hydrocephalic pigs at sacrifice (Fig. 2). MRI showed a reduction of the hippocampal volume in hydrocephalic pigs (Fig. 2A). The cross-sectional areas of the entire dorsal and ventral hippocampi were quantified as shown in Fig. 2B. Interestingly, the dorsal hippocampal area was significantly reduced by 23.4 % in hydrocephalic pigs compared with sham control pigs (**p=0.04, Mann-Whitney test) (Fig. 2C, D). No significant correlations were found between the decrease in hippocampal area and the increase in the size of the total ventricular system or the different parts of the lateral ventricles in hydrocephalic pigs (Supplemental Fig. 2).

The thickness of the layers of the hippocampus in CA1 was similar between both groups (Fig. 2E–G), except for the granular layer of the dorsal hippocampus which significantly increased by 17.8 % in the hydrocephalic pigs (p=0.004, Mann-Whitney test) (Fig. 2E`, F`).

Neurogenesis in the SGZ of the juvenile hippocampus

Neurogenesis, evaluated with DCX immunostaining, was analyzed in the dentate gyrus of the dorsal and ventral hippocampus in both groups at sacrifice. Three regions of interest containing the granular layer and the SGZ were used for quantification (Fig. 3A). In hydrocephalic pigs, the percentage of DCX+ cells was decreased by 32.4 % in the dentate gyrus of the dorsal hippocampus (3.1 ± 1.2 % vs. 1.7 ± 0.5 %; p=0.008, Mann-Whitney test) (Fig. 3B–D). Following the same trend, the percentage of mature neurons (NeuN+ cells) was decreased by 19.7% in the same locations (78.7 ± 5.4 % vs. 62.9 ± 11.5 %; p=0.008, Mann-Whitney test) (Fig. 3E–G).

Astrocytes and microglia in granular layer and hilus of the dorsal and ventral hippocampus

The number of reactive astrocytes (vimentin+ cells) and microglia (Iba1+ cells) were also quantified in the granular and SGZ of the dentate gyrus at sacrifice (Fig. 4). Interestingly, the percentage of reactive astrocytes was increased by 48.7 % in the granular/SGZ of the dorsal hippocampus in hydrocephalic pigs compared to sham pigs (2.4 ± 0.7 % sham vs. 3.5 ± 0.9 % hydro, vimentin+ cells) (p=0.041, Mann-Whitney Test) (Fig. 4A–C). The ventral hippocampus showed a similar percentage of vimentin+ cells in hydrocephalic pigs and sham pigs. Opposite to the astrocyte reaction, the percentage of microglial cells was found to decrease by 55.7 % in the granular/SGZ of the dorsal hippocampus in the hydrocephalic pigs (3.6 ± 1.3 %) compared to sham control pigs (6.2 ± 1.4 %) (p=0.014 Mann-Whitney Test) (Fig. 4D–G`).

No correlations were found between the hippocampal area and the percentage of all the analyzed cells (DCX, NeuN, vimentin, Iba1), except Iba1+ cells in the dorsal hippocampus (R^2=0.82, p=0.005, Simple linear regression) (Supplemental Fig. 3).

Behavioral and cognitive assessment

Behavioral and cognitive testing was performed prior to and one week after induction as described in the material and methods and shown in Supplemental Figure 4. Table 2 depicts general exploratory measures comparing pre-induction and post-induction periods in hydrocephalic pigs. Overall, there was no difference between RI at either time-point as indicated by $p > 0.05$, although some animals showed a decrease in RI (Supplemental Fig. 5). Differences were seen in object visit time and mean object visit time for the novel object (p=0.009, p=0.007, respectively, ANOVA), sample object (p=0.009, p=0.007), and both objects (p=0.002, p=0.002) when comparing pre-induction and post-induction among hydrocephalic pigs (Table 2).

Total and dorsal hippocampal width and length were measured after behavioral testing using MRI to analyze their possible association with recognition memory (14 ± 4 days post-induction, mean age of 58.9 days) (Fig. 5A). The hippocampal width was significantly reduced in hydrocephalic pigs (Fig. 5B), and significantly correlated with the increase in ventricular volume (R^2=0.39, p=0.03, simple linear regression, Fig. 5C). However, no correlations were found between the percent change of RI and either ventricular size or hippocampal width in hydrocephalic pigs (Supplemental Fig. 5). Furthermore, perirhinal cortex thickness was measured at the same time point (one week after the induction of hydrocephalus) using MRI, and significantly reduced cortex thickness was detected (sham mean 4.4 ± 0.6 mm and hydrocephalic mean 2.7 ± 0.3 mm; p=0.0003, Mann-Whitney test). Nevertheless, no correlations were found between perirhinal cortex thickness and RI percent change (R^2=0.03, p=0.58).

DISCUSSION

The present investigation aimed to analyze hippocampal and recognition memory alterations in a juvenile pig model of hydrocephalus. The dorsal hippocampus was reduced in size

in hydrocephalic pigs, accompanied by a decrease in the percentage of neuronal precursor cells (DCX+) and mature neurons in the granular layer and SGZ, and an increase in the number of reactive astrocytes. This hippocampal reduction was associated with the increase in ventricular volume. However, behavioral analysis revealed no significant differences in RI and no correlation with hippocampal size or perirhinal cortex thickness one week after the induction of hydrocephalus.

As previously described, we have developed a pig model of acquired hydrocephalus via a kaolin injection into the cisterna magna (McAllister et al., 2021; Garcia-Bonilla et al., 2022). This less invasive and consistent technique (Curzio, 2018) is a well-characterized method to induce hydrocephalus that has been widely used in rodents and large animals (Weller et al., 1971; Eskandari et al., 2004; Bloch et al., 2006; Khan et al., 2006; Li et al., 2008; Lopes Lda et al., 2009; Cardoso et al., 2011; Eskandari et al., 2011; Di Curzio et al., 2013; Johnston et al., 2013; Olopade et al., 2019). Ventriculomegaly was detected throughout the brain ventricular system and communication between the ventricles was maintained, although MRI images suggested restricted flow into the subarachnoid space (McAllister et al., 2021). The development of a large animal model for investigating the molecular mechanisms and sequelae of existing treatments for hydrocephalus can have a great impact on preclinical studies, even if it is logistically and financially challenging. We acknowledge the inherent variability in the progression and severity of hydrocephalus, but the challenging logistics for frequent post-induction evaluations resulted in a range of age and survival periods during the timeframe of this investigation. Nevertheless, our previous descriptions of this model (McAllister et al., 2021; Garcia-Bonilla et al., 2022) indicate that significant hydrocephalus occurs within the survival periods used in this study.

The neurodevelopment of the domestic pig brain is similar to the human brain (Dickerson and Dobbing, 1967; Dobbing and Sands, 1979; Conrad et al., 2012; Conrad and Johnson, 2015), and the postnatal period correlates with human development (Pond et al., 2000; Lind et al., 2007). The patterns of postnatal neurogenesis, neural differentiation, and myelination are very similar (Jelsing et al., 2006). In the age range of the pigs used in this work, the brain volume increases to 50 % of adult values, while 95 % is achieved at a later age (21–23 weeks) (Conrad et al., 2012; Conrad and Johnson, 2015).

Several studies have demonstrated that the hippocampus, medial prefrontal cortex, and perirhinal cortex establish a large network involved in recognition memory (Warburton and Brown, 2010; Wang et al., 2021). Furthermore, hippocampal impairments have resulted in changes in the recognition of a novel object in humans and monkeys (McKee and Squire, 1993; Nemanic et al., 2004; Squire et al., 2007; Broadbent et al., 2010) and rodents (Broadbent et al., 2010; Munyon et al., 2014; Arias et al., 2015). In children and animal models of hydrocephalus (Del Bigio et al., 2003; Di Curzio et al., 2018; Femi-Akinlosotu and Shokunbi, 2020; Femi-Akinlosotu et al., 2021), impaired cognitive function has been described impacting attention, executive memory, short-term memory, visual, spatial, and/or linguistic functionality, as well as behavioral issues (Bugalho et al., 2014; Zielińska et al., 2017; Wall et al., 2021). However, the literature is inconclusive about the association between larger ventricular size, smaller hippocampi and poorer cognitive and memory outcomes in hydrocephalus (Strahle et al., 2019; Riva-Cambrin et al., 2021). These findings

are in accordance with our results regarding lack of RI changes and lack of association with the increase in ventricular size or reduction of hippocampal and perirhinal cortex sizes. While the volume changes of different structures of the brain, including the ventricles, cortex, and hippocampus, have been associated with cognitive and neuropsychiatric changes (Fletcher et al., 1992; Kulkarni et al., 2010; Peterson et al., 2019; Strahle et al., 2019); other investigations have not found associations between treated ventricular size and cognitive outcomes (Azab et al., 2016; Riva-Cambrin et al., 2021). What seems to be clearer is the reduction in size and thickness of the hippocampus and its association with the increase in ventricular volume, as described in rodent models with different forms of hydrocephalus (Taveira et al., 2012; Chen et al., 2017; Femi-Akinlosotu et al., 2021) along with our pig model, in which reductions are more pronounced in the pyramidal layer in the CA1 region more than in the CA3 region (Taveira et al., 2012; Chen et al., 2017). Although the present study suggests that there is no association between cognition and ventricular or hippocampal size one week after the induction of hydrocephalus, it is possible that longer periods without treatment could result in cognitive deficits. Additional studies are needed to elucidate these cognitive changes in a long-term survival experiment of untreated hydrocephalus. Our future analyses will also include shunted pigs and cases with endoscopic third ventriculostomy with choroid plexus cauterization to evaluate neurobiological changes and cognitive function after treatment.

To our knowledge, this is the first time the cognition assessment has been applied to a juvenile large model of acquired hydrocephalus. The lack of RI changes in this pig model may be impacted by the neurodevelopmental juvenile stage of the brain (Conrad et al., 2012; Fleming and Dilger, 2017), and future studies will include pigs in earlier stages of development to analyze behavioral changes during neurodevelopment in acquired hydrocephalus. Additionally, we have observed that pigs during their initial round of testing appear more agitated and stressed, relative to subsequent rounds of testing, and it is possible that this can impact the overall exploration of the objects and the testing environment. Finally, the lack of significant differences found in the RI after the induction of hydrocephalus could be due to the relatively short time (one week) between the kaolin induction and cognitive testing; this period differs from our 30-day cellular analyses in which reduced neuronal progenitor cells and neuroinflammation were observed. Further studies will be conducted to assess cognition after more time post-induction. Another explanation for the lack of differences in RI could be related to the involvement of overlapping networks of the hippocampus and perirhinal cortex for components of both spatial and recognition memory (Burgess et al., 2002; Vann and Albasser, 2011). It is possible that, if spatial features are emphasized by using behavioral tests that combine aspects of spatial and object memories (Vann and Albasser, 2011), differences in RI could be detected in our pig model based on the cellular alterations observed in the hippocampus. Future tests, especially with more developmental and maturation timepoints, will include this approach to emphasize the importance of interactions between brain structures and types of memories rather than simple dissociations.

Neural progenitor cells are present in two regions of the brain: the subventricular zone proximal to the dorsolateral wall of the lateral ventricles and the SGZ of the dentate gyrus in the hippocampus (Wan et al., 2016). Several studies have demonstrated that a deficit of

hippocampal neurogenesis can lead to defective spatial learning and memory (Lee and Son, 2009; Lieberwirth et al., 2016; Alam et al., 2018), which may be related to environmental factors or intrinsic factors, such as neurotrophic factors, neurotransmitters, or steroids (Lieberwirth et al., 2016). For instance, brain-derived neurotrophic factor (BDNF) has been suggested to promote the survival of newborn neurons (Lee and Son, 2009) in various disorders including intraventricular hemorrhage and posthemorrhagic hydrocephalus (Ahn et al., 2021). In this porcine model, the loss of hippocampal and perirhinal cortex sizes and density of neuronal progenitor cells and neurons could be due to the increase in ventricular volume and intracranial pressure or CSF pulsatility, which displaces intraparenchymal fluid and consequently reduces brain tissue volume (Chen et al., 2017). Also, stretch and compression due to CSF accumulation and expansion of the ventricular system, especially in the temporal horn of the lateral ventricle close to the hippocampus and perirhinal cortex locations, could cause cell death (McAllister and Chovan, 1998). When ventricular dilation is mild, as observed in some of our cases, another explanation for this cellular loss could be the destruction of the fimbria-fornix connections rather than the effect of ventricular expansion over the hippocampus itself (Del Bigio et al., 2003; Taveira et al., 2012). Although we have detected statistically-significant size and cellular changes in the dorsal hippocampus, their magnitude may not be functionally and significantly correlated with recognition memory alterations. Moreover, the perirhinal cortex may show cellular changes as suggested by the reduction in thickness one week after induction. This size reduction may be related to the great expansion of the temporal horn of the lateral ventricles in this porcine model (Garcia-Bonilla et al., 2022), and further analyses will be carried out to understand the possible extension of these cellular changes. Finally, we acknowledge that the age difference might influence the hippocampus cross-sectional area, but its normalization with total brain volume was carried out to eliminate the brain size effect associated with age. Additionally, at 14 ± 4 days post-induction comparing animals of similar ages, hippocampal width was still significantly decreased in hydrocephalic pigs compared with sham controls.

Neuroinflammation in the dentate gyrus has also been associated with memory impairment and deterioration of adult neurogenesis (Wadhwa et al., 2019). An upregulation in the levels of different complement components, such as C3 or C5, has been described to decrease neurogenesis, while the use of antagonists for these components have improved adult neurogenesis via BDNF (Wadhwa et al., 2019). TNF alpha, a well-known inflammatory factor increased in hydrocephalus (Jiménez et al., 2014; Habiyaremye et al., 2017; Harris et al., 2021), has been also described to mediate necroptosis, resulting in neuronal loss in human cases with Alzheimer disease (Jayaraman et al., 2021). Thus, it is likely that neuroinflammation, present in the dorsal hippocampus through the increase of the number of reactive astrocytes (vimentin+ cells) in the dentate gyrus and of proinflammatory interleukins (IL6, IL8, TNF alpha) in the CSF as we have previously described in this model (Garcia-Bonilla et al., 2022) and in human cases (Habiyaremye et al., 2017; Morales et al., 2017), could be contributing to the hippocampal impairment and the increase of the granular layer thickness. Furthermore, ischemic conditions could be present in the hippocampus because of high intraventricular pressure (Del Bigio, 2000; Klinge et al., 2003), which can induce TNF alpha upregulation (Maddahi et al., 2011; Watters and O'Connor, 2011), and thus exacerbates neuroinflammation, astrocytosis, and its associated damages (Jiménez et

al., 2014). It is unclear why there was a reduction of microglial cells in hydrocephalic pigs, but it is possible that reactive microgliosis occurred earlier and was missed in our 30-day survival tissue, or that microglia may have migrated to more injured areas of the brain (Kettenmann et al., 2011; Ho, 2019) such as the periventricular white matter (Garcia-Bonilla et al., 2022). Recent evidence demonstrates that microglia can regulate neuronal postnatal development through the secretion of factors that modulate neurogenesis in neonatal and adult hippocampi (Soch et al., 2020; Chintamen et al., 2021) and SVZ (Shigemoto-Mogami et al., 2014). An increasing number of investigations have shown that microglial cells are implicated, not only in neuronal proliferation and differentiation, but also in synaptic connectivity, thereby influencing cognitive and behavioral functions (Al-Onaizi et al., 2020). Under neuroinflammatory conditions, microglial cells can release pro-inflammatory cytokines, such as IL6, IL1β, or TNF alpha, and induce a decrease in the production of new neurons (Pérez-Rodríguez et al., 2021). We have shown that IL6 is elevated in pigs with untreated hydrocephalus (Garcia-Bonilla et al., 2022); thus, it may be possible that the reduction of microglial cells observed in this pig model of hydrocephalus can be related to the reduction of hippocampal neurogenesis. Future studies will be conducted to explore this mechanism.

In conclusion, this study focused on analyzing the hippocampal and recognition memory changes associated with acquired hydrocephalus in juvenile pigs. Acquired hydrocephalus was accompanied by dorsal hippocampal size and perirhinal cortex thickness reduction, decreased neurogenesis in the SGZ, mature neurons in the granular layer, and astroglial activation. This model can be a useful tool for preclinical studies such as investigating the effects of current treatments on cognition and memory sequelae.

Supplementary Material

Refer to Web version on PubMed Central for supplementary material.

ACKNOWLEDGMENTS

We want to thank Todd Pavek for his veterinary support; Charles Mitchell, Angela Lewis, Matthew Bledsoe, Christopher Sanders, Troy Ingram and Zach Wellborn, for their logistical and surgical support in the Division of Comparative Medicine at the Washington University School of Medicine. Also, we are grateful for Linda Hood, Facility Manager & MRI Technologist, Department of Radiology-Research Entities, and Wilnellys Moore, MRI Technologist, for performing the MRI scans.

FUNDING

This work was supported by NIH 5R21NS111249-02 (JPM & DDL).

ABBREVIATIONS

CSF	cerebrospinal fluid
DAPI	4′,6-Diamidino-2-phenylindole dihydrochloride
DCX	doublecortin
Iba1	ionized calcium binding adaptor molecule 1

MRI	magnetic resonance imaging
NOR	novel object recognition
PBS	phosphate buffered saline
RI	recognition index
SD	standard deviation
SGZ	subgranular zone

REFERENCES

Ahn SY, Sung DK, Kim YE, Sung S, Chang YS, Park WS (2021) Brain-derived neurotropic factor mediates neuroprotection of mesenchymal stem cell-derived extracellular vesicles against severe intraventricular hemorrhage in newborn rats. Stem Cells Transl Med 10:374–384. [PubMed: 33319929]

Al-Onaizi M, Al-Khalifah A, Qasem D, ElAli A (2020) Role of Microglia in Modulating Adult Neurogenesis in Health and Neurodegeneration. International journal of molecular sciences 21.

Alam MJ, Kitamura T, Saitoh Y, Ohkawa N, Kondo T, Inokuchi K (2018) Adult Neurogenesis Conserves Hippocampal Memory Capacity. The Journal of neuroscience : the official journal of the Society for Neuroscience 38:6854–6863. [PubMed: 29986876]

Arias N, Méndez M, Arias JL (2015) The recognition of a novel-object in a novel context leads to hippocampal and parahippocampal c-Fos involvement. Behav Brain Res 292:44–49. [PubMed: 26072392]

Azab WA, Mijalcic RM, Nakhi SB, Mohammad MH (2016) Ventricular volume and neurocognitive outcome after endoscopic third ventriculostomy: is shunting a better option? A review. Child's nervous system 32:775–780.

Barker GRI, Warburton EC (2011) When Is the Hippocampus Involved in Recognition Memory? The Journal of Neuroscience 31:10721–10731. [PubMed: 21775615]

Bloch O, Auguste KI, Manley GT, Verkman AS (2006) Accelerated progression of kaolin-induced hydrocephalus in aquaporin-4-deficient mice. Journal of cerebral blood flow and metabolism 26:1527–1537. [PubMed: 16552421]

Bouyeure A, Germanaud D, Bekha D, Delattre V, Lefèvre J, Pinabiaux C, Mangin J-F, Rivière D, Fischer C, Chiron C, Hertz-Pannier L, Noulhiane M (2018) Three-Dimensional Probabilistic Maps of Mesial Temporal Lobe Structures in Children and Adolescents' Brains. Frontiers in Neuroanatomy 12.

Broadbent NJ, Gaskin S, Squire LR, Clark RE (2010) Object recognition memory and the rodent hippocampus. Learn Mem 17:5–11. [PubMed: 20028732]

Bugalho P, Alves L, Miguel R, Ribeiro O (2014) Profile of cognitive dysfunction and relation with gait disturbance in Normal Pressure Hydrocephalus. Clin Neurol Neurosurg 118:83–88. [PubMed: 24529236]

Burgess N, Maguire EA, O'Keefe J (2002) The human hippocampus and spatial and episodic memory. Neuron 35:625–641. [PubMed: 12194864]

Cardoso EJ, Lachat JJ, Lopes LS, Santos AC, Colli BO (2011) Changes caused by hydrocephalus, induced by kaolin, in the corpus callosum of adult dogs. Acta Cir Bras 26 Suppl 2:8–14.

Chaudhry SR, Stoffel-Wagner B, Kinfe TM, Güresir E, Vatter H, Dietrich D, Lamprecht A, Muhammad S (2017) Elevated Systemic IL-6 Levels in Patients with Aneurysmal Subarachnoid Hemorrhage Is an Unspecific Marker for Post-SAH Complications. International journal of molecular sciences 18.

Chen LJ, Wang YJ, Chen JR, Tseng GF (2017) Hydrocephalus compacted cortex and hippocampus and altered their output neurons in association with spatial learning and memory deficits in rats. Brain Pathol 27:419–436. [PubMed: 27411167]

Chintamen S, Imessadouene F, Kernie SG (2021) Immune Regulation of Adult Neurogenic Niches in Health and Disease. Frontiers in Cellular Neuroscience 14.

Conrad MS, Johnson RW (2015) The domestic piglet: an important model for investigating the neurodevelopmental consequences of early life insults. Annu Rev Anim Biosci 3:245–264. [PubMed: 25387115]

Conrad MS, Dilger RN, Johnson RW (2012) Brain growth of the domestic pig (Sus scrofa) from 2 to 24 weeks of age: a longitudinal MRI study. Developmental neuroscience 34:291–298. [PubMed: 22777003]

Coulter IC et al. (2020) Cranial and ventricular size following shunting or endoscopic third ventriculostomy (ETV) in infants with aqueductal stenosis: further insights from the International Infant Hydrocephalus Study (IIHS). Child's nervous system 36:1407–1414.

Curzio DLD (2018) Animal Models of Hydrocephalus. Open Journal of Modern Neurosurgery Vol.08No.01:14.

Czubowicz K, Głowacki M, Fersten E, Kozłowska E, Strosznajder RP, Czernicki Z (2017) Levels of selected pro- and anti-inflammatory cytokines in cerebrospinal fluid in patients with hydrocephalus. Folia neuropathologica 55:301–307. [PubMed: 29363904]

da Silva MC (2005) Pathophysiology of Hydrocephalus. In: Pediatric Hydrocephalus (Cinalli G, Sainte-Rose C, Maixner WJ, eds), pp 65–77. Milano: Springer Milan.

Del Bigio MR (2000) Calcium-mediated proteolytic damage in white matter of hydrocephalic rats? Journal of neuropathology and experimental neurology 59:946–954. [PubMed: 11089572]

Del Bigio MR (2010) Neuropathology and structural changes in hydrocephalus. Developmental disabilities research reviews 16:16–22. [PubMed: 20419767]

Del Bigio MR, Wilson MJ, Enno T (2003) Chronic hydrocephalus in rats and humans: white matter loss and behavior changes. Annals of neurology 53:337–346. [PubMed: 12601701]

Di Curzio DL, Buist RJ, Del Bigio MR (2013) Reduced subventricular zone proliferation and white matter damage in juvenile ferrets with kaolin-induced hydrocephalus. Experimental neurology 248:112–128. [PubMed: 23769908]

Di Curzio DL, Mao X, Baker A, Del Bigio MR (2018) Nimodipine treatment does not benefit juvenile ferrets with kaolin-induced hydrocephalus. Fluids and barriers of the CNS 15:14. [PubMed: 29720231]

Dickerson JW, Dobbing J (1967) Prenatal and postnatal growth and development of the central nervous system of the pig. Proc R Soc Lond B Biol Sci 166:384–395. [PubMed: 24796035]

Dilger RN, Johnson RW (2010) Behavioral assessment of cognitive function using a translational neonatal piglet model. Brain Behav Immun 24:1156–1165. [PubMed: 20685307]

Dobbing J, Sands J (1979) Comparative aspects of the brain growth spurt. Early Hum Dev 3:79–83. [PubMed: 118862]

Domínguez-Pinos MD, Páez P, Jiménez AJ, Weil B, Arráez MA, Pérez-Fígares JM, Rodríguez EM (2005) Ependymal denudation and alterations of the subventricular zone occur in human fetuses with a moderate communicating hydrocephalus. Journal of neuropathology and experimental neurology 64:595–604. [PubMed: 16042311]

Erickson K, Baron IS, Fantie BD (2001) Neuropsychological functioning in early hydrocephalus: review from a developmental perspective. Child Neuropsychol 7:199–229. [PubMed: 16210211]

Eskandari R, Harris CA, McAllister JP 2nd (2011) Reactive astrocytosis in feline neonatal hydrocephalus: acute, chronic, and shunt-induced changes. Child's nervous system 27:2067–2076.

Eskandari R, McAllister JP 2nd, Miller JM, Ding Y, Ham SD, Shearer DM, Way JS (2004) Effects of hydrocephalus and ventriculoperitoneal shunt therapy on afferent and efferent connections in the feline sensorimotor cortex. Journal of neurosurgery 101:196–210. [PubMed: 15835108]

Fares J, Bou Diab Z, Nabha S, Fares Y (2019) Neurogenesis in the adult hippocampus: history, regulation, and prospective roles. Int J Neurosci 129:598–611. [PubMed: 30433866]

Femi-Akinlosotu OM, Shokunbi MT (2020) Changes in Neuronal Density of the Sensorimotor Cortex and Neurodevelopmental Behaviour in Neonatal Mice with Kaolin-Induced Hydrocephalus. Pediatric neurosurgery 55:244–253. [PubMed: 33108787]

Femi-Akinlosotu OM, Shokunbi MT, Olopade FE, Igbong P (2021) Deficits of Learning and Spatial Memory are Associated with Increased Pyknosis of Pyramidal Neurons of the Hippocampus of Adult Rats with Chronic Hydrocephalus. West Afr J Med Vol. 38:1042–1049.

Fleming SA, Dilger RN (2017) Young pigs exhibit differential exploratory behavior during novelty preference tasks in response to age, sex, and delay. Behav Brain Res 321:50–60. [PubMed: 28042005]

Fleming SA, Monaikul S, Patsavas AJ, Waworuntu RV, Berg BM, Dilger RN (2019) Dietary polydextrose and galactooligosaccharide increase exploratory behavior, improve recognition memory, and alter neurochemistry in the young pig. Nutr Neurosci 22:499–512. [PubMed: 29251222]

Fletcher JM, Bohan TP, Brandt ME, Brookshire BL, Beaver SR, Francis DJ, Davidson KC, Thompson NM, Miner ME (1992) Cerebral white matter and cognition in hydrocephalic children. Arch Neurol 49:818–824. [PubMed: 1524514]

Furey CG, Antwi Prince, and Kahle Kristopher T (2019) Congenital Hydrocephalus. In: Cerebrospinal Fluid Disorders, 1 Edition (Leonard DDJLaJ, ed), pp 87–113: Springer International Publishing.

Garcia-Bonilla M, McAllister JP, Limbrick DD (2021) Genetics and Molecular Pathogenesis of Human Hydrocephalus. Neurol India 69:S268–s274. [PubMed: 35102976]

Garcia-Bonilla M, Castaneyra-Ruiz L, Zwick S, Talcott M, Otun A, Isaacs AM, Morales DM, Limbrick DD Jr., McAllister JP 2nd (2022) Acquired hydrocephalus is associated with neuroinflammation, progenitor loss, and cellular changes in the subventricular zone and periventricular white matter. Fluids and barriers of the CNS 19:17. [PubMed: 35193620]

Garton TP, He Y, Garton HJ, Keep RF, Xi G, Strahle JM (2016) Hemoglobin-induced neuronal degeneration in the hippocampus after neonatal intraventricular hemorrhage. Brain research 1635:86–94. [PubMed: 26772987]

Goulding DS, Vogel RC, Pandya CD, Shula C, Gensel JC, Mangano FT, Goto J, Miller BA (2020) Neonatal hydrocephalus leads to white matter neuroinflammation and injury in the corpus callosum of Ccdc39 hydrocephalic mice. Journal of neurosurgery Pediatrics:1–8.

Gram M, Sveinsdottir S, Ruscher K, Hansson SR, Cinthio M, Akerström B, Ley D (2013) Hemoglobin induces inflammation after preterm intraventricular hemorrhage by methemoglobin formation. Journal of neuroinflammation 10:100. [PubMed: 23915174]

Guerra MM, Henzi R, Ortloff A, Lichtin N, Vío K, Jiménez AJ, Dominguez-Pinos MD, González C, Jara MC, Hinostroza F, Rodríguez S, Jara M, Ortega E, Guerra F, Sival DA, den Dunnen WF, Pérez-Fígares JM, McAllister JP, Johanson CE, Rodríguez EM (2015) Cell Junction Pathology of Neural Stem Cells Is Associated With Ventricular Zone Disruption, Hydrocephalus, and Abnormal Neurogenesis. Journal of neuropathology and experimental neurology 74:653–671. [PubMed: 26079447]

Habiyaremye G, Morales DM, Morgan CD, McAllister JP, CreveCoeur TS, Han RH, Gabir M, Baksh B, Mercer D, Limbrick DD Jr. (2017) Chemokine and cytokine levels in the lumbar cerebrospinal fluid of preterm infants with post-hemorrhagic hydrocephalus. Fluids and barriers of the CNS 14:35. [PubMed: 29228970]

Harris CA, Morales DM, Arshad R, McAllister JP 2nd, Limbrick DD Jr. (2021) Cerebrospinal fluid biomarkers of neuroinflammation in children with hydrocephalus and shunt malfunction. Fluids and barriers of the CNS 18:4. [PubMed: 33514409]

Ho MS (2019) Microglia in Parkinson's Disease. Adv Exp Med Biol 1175:335–353. [PubMed: 31583594]

Isaacs AM, Riva-Cambrin J, Yavin D, Hockley A, Pringsheim TM, Jette N, Lethebe BC, Lowerison M, Dronyk J, Hamilton MG (2018) Age-specific global epidemiology of hydrocephalus: Systematic review, metanalysis and global birth surveillance. PloS one 13:e0204926. [PubMed: 30273390]

Jayaraman A, Htike TT, James R, Picon C, Reynolds R (2021) TNF-mediated neuroinflammation is linked to neuronal necroptosis in Alzheimer's disease hippocampus. Acta Neuropathol Commun 9:159. [PubMed: 34625123]

Jelsing J, Nielsen R, Olsen AK, Grand N, Hemmingsen R, Pakkenberg B (2006) The postnatal development of neocortical neurons and glial cells in the Göttingen minipig and the domestic pig brain. J Exp Biol 209:1454–1462. [PubMed: 16574805]

Jiménez AJ, García-Verdugo JM, González CA, Bátiz LF, Rodríguez-Pérez LM, Páez P, Soriano-Navarro M, Roales-Buján R, Rivera P, Rodríguez S, Rodríguez EM, Pérez-Fígares JM (2009) Disruption of the neurogenic niche in the subventricular zone of postnatal hydrocephalic hyh mice. Journal of neuropathology and experimental neurology 68:1006–1020. [PubMed: 19680142]

Jiménez AJ, Rodríguez-Pérez LM, Domínguez-Pinos MD, Gómez-Roldán MC, GarcíaBonilla M, Ho-Plagaro A, Roales-Buján R, Jiménez S, Roquero-Mañueco MC, Martínez-León MI, García-Martín ML, Cifuentes M, Ros B, Arráez M, Vitorica J, Gutiérrez A, Pérez-Fígares JM (2014) Increased levels of tumour necrosis factor alpha (TNFα) but not transforming growth factor-beta 1 (TGFβ1) are associated with the severity of congenital hydrocephalus in the hyh mouse. Neuropathology and applied neurobiology 40:911–932. [PubMed: 24707814]

Johnston MG, Del Bigio MR, Drake JM, Armstrong D, Di Curzio DL, Bertrand J (2013) Pre- and post-shunting observations in adult sheep with kaolin-induced hydrocephalus. Fluids and barriers of the CNS 10:24. [PubMed: 23845003]

Jusué-Torres I, Jeon LH, Sankey EW, Lu J, Vivas-Buitrago T, Crawford JA, Pletnikov MV, Xu J, Blitz A, Herzka DA, Crain B, Hulbert A, Guerrero-Cazares H, Gonzalez-Perez O, McAllister JP 2nd, Quiñones-Hinojosa A, Rigamonti D (2016) A Novel Experimental Animal Model of Adult Chronic Hydrocephalus. Neurosurgery 79:746–756. [PubMed: 27759679]

Kahle KT, Kulkarni AV, Limbrick DD Jr., Warf BC (2016) Hydrocephalus in children. Lancet (London, England) 387:788–799. [PubMed: 26256071]

Karimy JK, Reeves BC, Damisah E, Duy PQ, Antwi P, David W, Wang K, Schiff SJ, Limbrick DD Jr., Alper SL, Warf BC, Nedergaard M, Simard JM, Kahle KT (2020) Inflammation in acquired hydrocephalus: pathogenic mechanisms and therapeutic targets. Nature reviews Neurology 16:285–296. [PubMed: 32152460]

Kempermann G, Song H, Gage FH (2015) Neurogenesis in the Adult Hippocampus. Cold Spring Harb Perspect Biol 7:a018812. [PubMed: 26330519]

Kettenmann H, Hanisch UK, Noda M, Verkhratsky A (2011) Physiology of microglia. Physiol Rev 91:461–553. [PubMed: 21527731]

Khan OH, Del Bigio MR (2006) Experimental models of hydrocephalus. In: Handbook of Experimental Neurology: Methods and Techniques in Animal Research (Fisher M, Tatlisumak T, eds), pp 457–471. Cambridge: Cambridge University Press.

Khan OH, Enno TL, Del Bigio MR (2006) Brain damage in neonatal rats following kaolin induction of hydrocephalus. Experimental neurology 200:311–320. [PubMed: 16624304]

Klinge PM, Samii A, Mühlendyck A, Visnyei K, Meyer GJ, Walter GF, Silverberg GD, Brinker T (2003) Cerebral hypoperfusion and delayed hippocampal response after induction of adult kaolin hydrocephalus. Stroke 34:193–199. [PubMed: 12511773]

Kriebel RM, McAllister JP 2nd (2000) Pathology of the hippocampus in experimental feline infantile hydrocephalus. Neurological research 22:29–36. [PubMed: 10672578]

Kulkarni AV, Hui S, Shams I, Donnelly R (2010) Quality of life in obstructive hydrocephalus: endoscopic third ventriculostomy compared to cerebrospinal fluid shunt. Child's nervous system 26:75–79.

Kulkarni AV, Riva-Cambrin J, Rozzelle CJ, Naftel RP, Alvey JS, Reeder RW, Holubkov R, Browd SR, Cochrane DD, Limbrick DD, Simon TD, Tamber M, Wellons JC, Whitehead WE, Kestle JRW (2018) Endoscopic third ventriculostomy and choroid plexus cauterization in infant hydrocephalus: a prospective study by the Hydrocephalus Clinical Research Network. Journal of neurosurgery Pediatrics 21:214–223. [PubMed: 29243972]

Lee E, Son H (2009) Adult hippocampal neurogenesis and related neurotrophic factors. BMB Rep 42:239–244. [PubMed: 19470236]

Li J, McAllister JP 2nd, Shen Y, Wagshul ME, Miller JM, Egnor MR, Johnston MG, Haacke EM, Walker ML (2008) Communicating hydrocephalus in adult rats with kaolin obstruction of the basal cisterns or the cortical subarachnoid space. Experimental neurology 211:351–361. [PubMed: 18433747]

Lieberwirth C, Pan Y, Liu Y, Zhang Z, Wang Z (2016) Hippocampal adult neurogenesis: Its regulation and potential role in spatial learning and memory. Brain research 1644:127–140. [PubMed: 27174001]

Lind NM, Moustgaard A, Jelsing J, Vajta G, Cumming P, Hansen AK (2007) The use of pigs in neuroscience: modeling brain disorders. Neuroscience and biobehavioral reviews 31:728–751. [PubMed: 17445892]

Lopes Lda S, Slobodian I, Del Bigio MR (2009) Characterization of juvenile and young adult mice following induction of hydrocephalus with kaolin. Experimental neurology 219:187–196. [PubMed: 19460371]

Maddahi A, Kruse LS, Chen QW, Edvinsson L (2011) The role of tumor necrosis factor-α and TNF-α receptors in cerebral arteries following cerebral ischemia in rat. Journal of neuroinflammation 8:107. [PubMed: 21871121]

Mangano FT, McAllister JP 2nd, Jones HC, Johnson MJ, Kriebel RM (1998) The microglial response to progressive hydrocephalus in a model of inherited aqueductal stenosis. Neurological research 20:697–704. [PubMed: 9864733]

McAllister JP, Talcott M, Isaacs AM, Zwick SH, Garcia-Bonilla M, Castaneyra-Ruiz L, Hartman A, Dilger RN, Fleming SA, Golden RK, Morales DM, Harris C, Limbrick DD (2021) A novel model of acquired hydrocephalus for evaluation of neurosurgical treatments. Fluids and barriers of the CNS 18:49. [PubMed: 34749745]

McAllister JP 2nd (2012) Pathophysiology of congenital and neonatal hydrocephalus. Seminars in fetal & neonatal medicine 17:285–294. [PubMed: 22800608]

McAllister JP 2nd, Chovan P (1998) Neonatal hydrocephalus. Mechanisms and consequences. Neurosurgery clinics of North America 9:73–93. [PubMed: 9405766]

McKee RD, Squire LR (1993) On the development of declarative memory. Journal of Experimental Psychology: Learning, Memory, and Cognition 19:397–404. [PubMed: 8454964]

Morales DM, Silver SA, Morgan CD, Mercer D, Inder TE, Holtzman DM, Wallendorf MJ, Rao R, McAllister JP, Limbrick DD Jr. (2017) Lumbar Cerebrospinal Fluid Biomarkers of Posthemorrhagic Hydrocephalus of Prematurity: Amyloid Precursor Protein, Soluble Amyloid Precursor Protein α, and L1 Cell Adhesion Molecule. Neurosurgery 80:82–90. [PubMed: 27571524]

Munyon C, Eakin KC, Sweet JA, Miller JP (2014) Decreased bursting and novel object-specific cell firing in the hippocampus after mild traumatic brain injury. Brain research 1582:220–226. [PubMed: 25086204]

Nemanic S, Alvarado MC, Bachevalier J (2004) The Hippocampal/Parahippocampal Regions and Recognition Memory: Insights from Visual Paired Comparison versus Object-Delayed Nonmatching in Monkeys. The Journal of Neuroscience 24:2013–2026. [PubMed: 14985444]

Olopade FE, Shokunbi MT, Azeez IA, Andrioli A, Scambi I, Bentivoglio M (2019) Neuroinflammatory Response in Chronic Hydrocephalus in Juvenile Rats. Neuroscience 419:14–22. [PubMed: 31491504]

Paturu M, Triplett RL, Thukral S, Alexopoulos D, Smyser CD, Limbrick DD, Strahle JM (2022) Does ventricle size contribute to cognitive outcomes in posthemorrhagic hydrocephalus? Role of early definitive intervention. Journal of neurosurgery Pediatrics 29:10–20. [PubMed: 34653990]

Pérez-Rodríguez DR, Blanco-Luquin I, Mendioroz M (2021) The Participation of Microglia in Neurogenesis: A Review. Brain Sciences 11:658. [PubMed: 34070012]

Peterson KA, Mole TB, Keong NCH, DeVito EE, Savulich G, Pickard JD, Sahakian BJ (2019) Structural correlates of cognitive impairment in normal pressure hydrocephalus. Acta Neurol Scand 139:305–312. [PubMed: 30428124]

Pindrik J et al. (2020) Surgical resource utilization after initial treatment of infant hydrocephalus: comparing ETV, early experience of ETV with choroid plexus cauterization, and shunt insertion in the Hydrocephalus Clinical Research Network. Journal of neurosurgery Pediatrics:1–9.

Pond WG, Boleman SL, Fiorotto ML, Ho H, Knabe DA, Mersmann HJ, Savell JW, Su DR (2000) Perinatal ontogeny of brain growth in the domestic pig. Proc Soc Exp Biol Med 223:102–108. [PubMed: 10632968]

Rekate HL (2011) A consensus on the classification of hydrocephalus: its utility in the assessment of abnormalities of cerebrospinal fluid dynamics. Child's nervous system 27:1535–1541.

Riva-Cambrin J, Kestle JRW, Rozzelle CJ, Naftel RP, Alvey JS, Reeder RW, Holubkov R, Browd SR, Cochrane DD, Limbrick DD, Shannon CN, Simon TD, Tamber MS, Wellons JC, Whitehead

WE, Kulkarni AV (2019) Predictors of success for combined endoscopic third ventriculostomy and choroid plexus cauterization in a North American setting: a Hydrocephalus Clinical Research Network study. Journal of neurosurgery Pediatrics 24:128–138. [PubMed: 31151098]

Riva-Cambrin J et al. (2021) Impact of ventricle size on neuropsychological outcomes in treated pediatric hydrocephalus: an HCRN prospective cohort study. Journal of neurosurgery Pediatrics:1–12.

Robinson S (2012) Neonatal posthemorrhagic hydrocephalus from prematurity: pathophysiology and current treatment concepts. Journal of neurosurgery Pediatrics 9:242–258. [PubMed: 22380952]

Sharma S, Goyal MK, Sharma K, Modi M, Sharma M, Khandelwal N, Prabhakar S, Sharma N, R S, Gairolla J, Jain A, Lal V (2017) Cytokines do play a role in pathogenesis of tuberculous meningitis: A prospective study from a tertiary care center in India. Journal of the neurological sciences 379:131–136. [PubMed: 28716226]

Shigemoto-Mogami Y, Hoshikawa K, Goldman JE, Sekino Y, Sato K (2014) Microglia enhance neurogenesis and oligodendrogenesis in the early postnatal subventricular zone. The Journal of neuroscience : the official journal of the Society for Neuroscience 34:2231–2243. [PubMed: 24501362]

Shirane R, Sato S, Sato K, Kameyama M, Ogawa A, Yoshimoto T, Hatazawa J, Ito M (1992) Cerebral blood flow and oxygen metabolism in infants with hydrocephalus. Child's nervous system 8:118–123.

Soch A, Sominsky L, Younesi S, De Luca SN, Gunasekara M, Bozinovski S, Spencer SJ (2020) The role of microglia in the second and third postnatal weeks of life in rat hippocampal development and memory. Brain, Behavior, and Immunity 88:675–687. [PubMed: 32360602]

Squire LR, Wixted JT, Clark RE (2007) Recognition memory and the medial temporal lobe: a new perspective. Nat Rev Neurosci 8:872–883. [PubMed: 17948032]

Strahle JM, Triplett RL, Alexopoulos D, Smyser TA, Rogers CE, Limbrick DD Jr., Smyser CD (2019) Impaired hippocampal development and outcomes in very preterm infants with perinatal brain injury. Neuroimage Clin 22:101787. [PubMed: 30991622]

Taveira KV, Carraro KT, Catalão CH, Lopes Lda S (2012) Morphological and morphometric analysis of the hippocampus in Wistar rats with experimental hydrocephalus. Pediatric neurosurgery 48:163–167. [PubMed: 23306373]

Tully HM, Dobyns WB (2014) Infantile hydrocephalus: a review of epidemiology, classification and causes. European journal of medical genetics 57:359–368. [PubMed: 24932902]

Turgut M, Baka M, Uyanıkgil Y (2018) Melatonin Attenuates Histopathological Changes in the Hippocampus of Infantile Rats with Kaolin-Induced Hydrocephalus. Pediatric neurosurgery 53:229–237. [PubMed: 29791910]

Tzakis N, Holahan MR (2019) Social Memory and the Role of the Hippocampal CA2 Region. Frontiers in Behavioral Neuroscience 13.

Vann SD, Albasser MM (2011) Hippocampus and neocortex: recognition and spatial memory. Curr Opin Neurobiol 21:440–445. [PubMed: 21353527]

Voss JL, Bridge DJ, Cohen NJ, Walker JA (2017) A Closer Look at the Hippocampus and Memory. Trends Cogn Sci 21:577–588. [PubMed: 28625353]

Wadhwa M, Prabhakar A, Anand JP, Ray K, Prasad D, Kumar B, Panjwani U (2019) Complement activation sustains neuroinflammation and deteriorates adult neurogenesis and spatial memory impairment in rat hippocampus following sleep deprivation. Brain Behav Immun 82:129–144. [PubMed: 31408672]

Wall VL, Kestle JRW, Fulton JB, Gale SD (2021) Social-emotional functioning in pediatric hydrocephalus: comparison of the Hydrocephalus Outcome Questionnaire to the Behavior Assessment System for Children. Journal of neurosurgery Pediatrics 28:572–578. [PubMed: 34416725]

Wan F, Bai HJ, Liu JQ, Tian M, Wang YX, Niu X, Si YC (2016) Proliferation and Glia-Directed Differentiation of Neural Stem Cells in the Subventricular Zone of the Lateral Ventricle and the Migratory Pathway to the Lesions after Cortical Devascularization of Adult Rats. BioMed research international 2016:3625959. [PubMed: 27294116]

Wang C, Furlong TM, Stratton PG, Lee CCY, Xu L, Merlin S, Nolan C, Arabzadeh E, Marek R, Sah P (2021) Hippocampus-Prefrontal Coupling Regulates Recognition Memory for Novelty Discrimination. The Journal of neuroscience : the official journal of the Society for Neuroscience 41:9617–9632. [PubMed: 34642213]

Warburton EC, Brown MW (2010) Findings from animals concerning when interactions between perirhinal cortex, hippocampus and medial prefrontal cortex are necessary for recognition memory. Neuropsychologia 48:2262–2272. [PubMed: 20026141]

Watters O, O'Connor JJ (2011) A role for tumor necrosis factor-α in ischemia and ischemic preconditioning. Journal of neuroinflammation 8:87. [PubMed: 21810263]

Weller RO, Wiśniewski H, Shulman K, Terry RD (1971) Experimental hydrocephalus in young dogs: histological and ultrastructural study of the brain tissue damage. Journal of neuropathology and experimental neurology 30:613–626. [PubMed: 5135016]

Wixey JA, Lee KM, Miller SM, Goasdoue K, Colditz PB, Tracey Bjorkman S, Chand KK (2019) Neuropathology in intrauterine growth restricted newborn piglets is associated with glial activation and proinflammatory status in the brain. Journal of neuroinflammation 16:5. [PubMed: 30621715]

Zhernovaia M, Dadar M, Mahmoud S, Zeighami Y, Maranzano J (2020) PhyloBrain atlas: a cortical brain MRI atlas following a phylogenetic approach.

Zielińska D, Rajtar-Zembaty A, Starowicz-Filip A (2017) Cognitive disorders in children's hydrocephalus. Neurol Neurochir Pol 51:234–239. [PubMed: 28284447]

HIGHLIGHTS

- Hippocampal area and width are reduced in acquired hydrocephalus
- Neurogenesis in dorsal subgranular zone is decreased in acquired hydrocephalus
- Mature neurons in dorsal granular zone are reduced in acquired hydrocephalus
- Reactive astrocytosis occurs in the dentate gyrus in acquired hydrocephalus
- No correlation between hippocampal size reduction and recognition memory

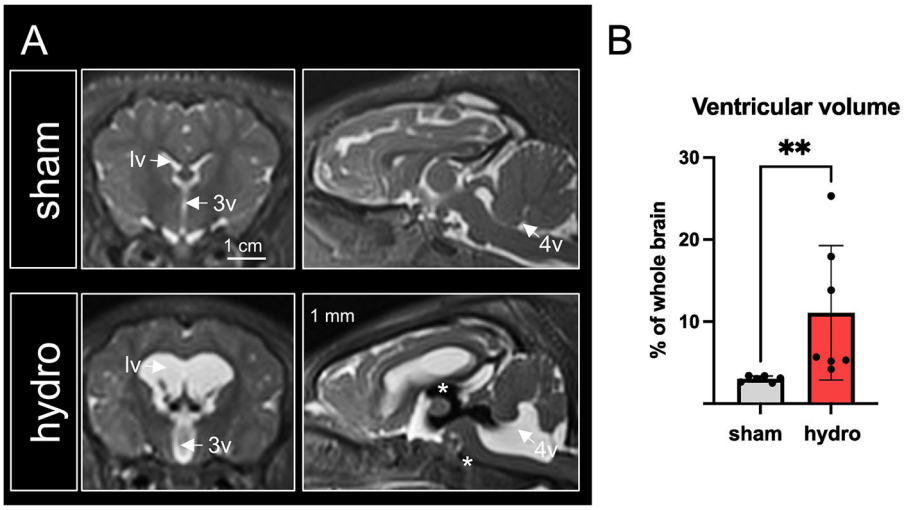

FIGURE 1. Ventricular dilation after the induction of hydrocephalus at sacrifice.

(**A**) Representative magnetic resonance images show the most pronounced increase of the lateral (*lv*), third (*3v*), and fourth (*4v*) ventricles from a sham control pig (top row) and a hydrocephalic pig (bottom row). CSF flow void is pointed with the top asterisk and CSF obstruction is pointed with the bottom asterisk in the hydrocephalic pig. Scales bars are identical for all panels. (**B**) Graph illustrating a significant increase in ventricular volume in hydrocephalic pigs (**p=0.0012, Mann-Whitney test).

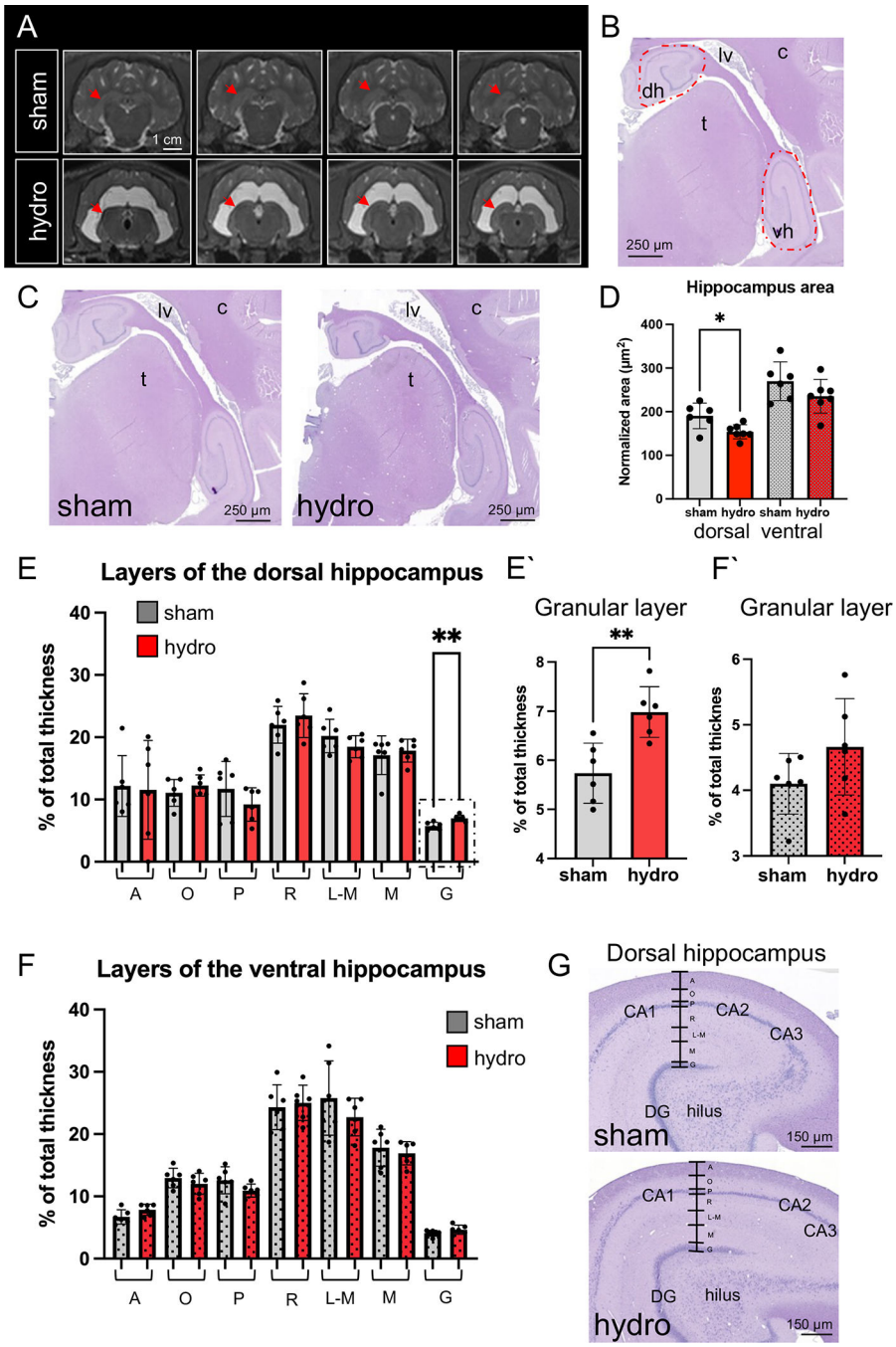

FIGURE 2. Hippocampal area reduction and thickness of the hippocampal layers at sacrifice.

(**A**) A smaller size of the hippocampus in hydrocephalic pigs was noticed in magnetic resonance imaging (red arrows). Four matched and serial images from anterior to posterior of a sham control pig (top row) and a hydrocephalic pig (bottom row) are shown. (**B**) Area quantification of the dorsal (*dh*) and ventral (*vh*) hippocampus was performed as shown with red dashed lines and adjusted by total brain volume. One of every sixty sections of the entire hippocampus was stained with hematoxylin-eosin for both groups. (**C**, **D**) The dorsal hippocampal cross-sectional area was significantly reduced in hydrocephalic pigs

compared to sham controls (**p=0.035, Mann-Whitney test). Area was normalized by total brain volume in each case. (**E-G**) The thickness of hippocampal layers in CA1 was similar in the dorsal and ventral hippocampus of both sham and hydrocephalic groups, with the exception that the granular layer was significantly thicker (**p=0.0043, Mann-Whitney test) in the dorsal hippocampus (**È**) compared to the ventral (**F`**) in the hydrocephalic pigs. Abbreviations: A, alveus layer; O, oriens layer; P, pyramidale layer; R, radiatum layer; L-M, lacunosum-moleculare layer; M, moleculare layer; G, granulosum layer; lv, lateral ventricle; t, thalamus; c, cortex; dg, dentate gyrus.

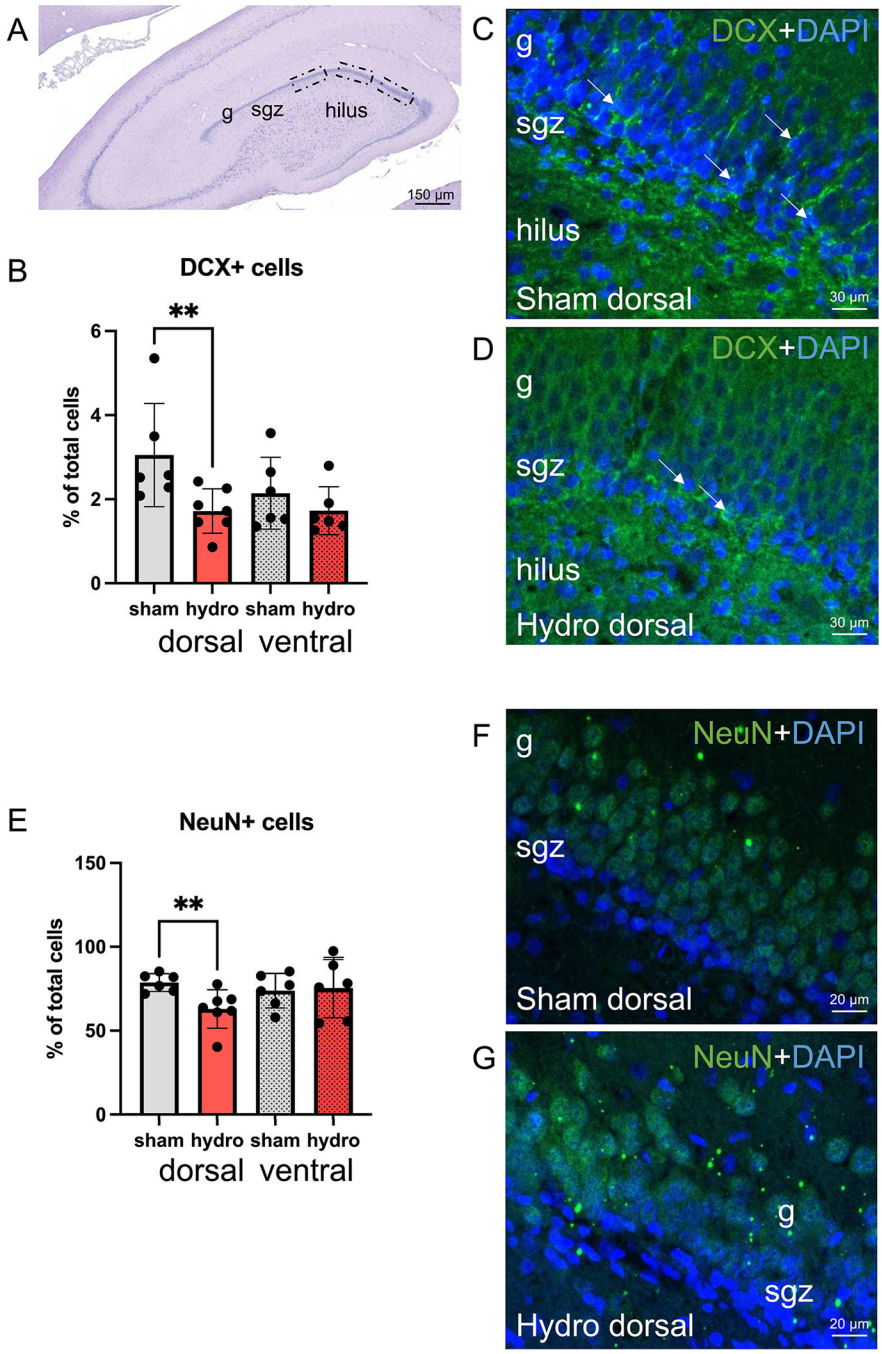

FIGURE 3. Reduced neurogenesis in the dentate gyrus of the dorsal hippocampus at sacrifice.

(A) Neurogenesis was quantified with doublecortin (DCX) immunostaining in the granular layer (*g*) and subgranular zone (*sgz*) of the dentate gyrus as shown in this hematoxylin-eosin staining picture (squared areas) of the dorsal hippocampus. (**B**) The density of DCX (*green*) positive cells (white arrows in **C** and **D**) was reduced in the granular layer and SGZ of the dorsal hippocampus in (**D**) hydrocephalic pigs compared with (**C**) sham control pigs (**p=0.0082, Mann-Whitney test). (**E**) Similarly, the percentage of mature neurons (NeuN, *green*) was decreased in the granular layer of the dorsal dentate gyrus in (**G**)

hydrocephalic pigs compared with (**F**) sham control pigs (**p=0.0082, Mann-Whitney test). The brightest dots are artifacts in **F** and **G**. Nuclear staining in blue with DAPI. Images were obtained under the confocal microscope, and a Z-stack of 10 μm was composed with ImageJ software.

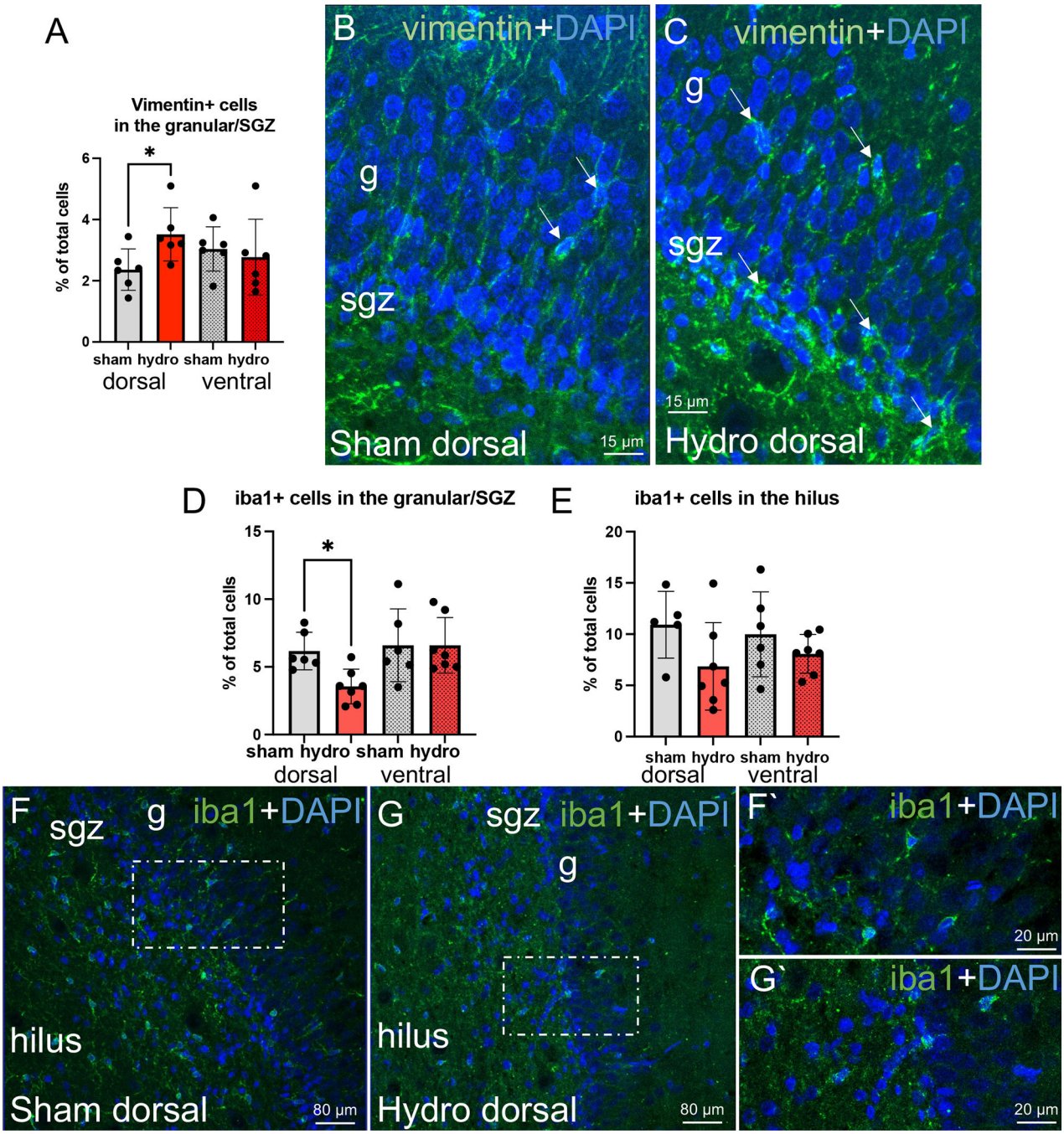

FIGURE 4. Neuroinflammation in the granular layer and subgranular zone (SGZ) of the dentate gyrus in the dorsal hippocampus at sacrifice.

(**A-C**) Vimentin immunostaining (*green*) confirmed the increase of reactive astrocytes in the granular/SGZ of the dorsal hippocampus in (**C**) hydrocephalic pigs compared to (**B**) sham pigs (p=0.0411 Mann-Whitney test). (**D, E**) However, the microglial reaction (Iba1, *green*) was significantly reduced in (**G**) hydrocephalic pigs compared with (**F**) sham control pigs in the granular and SGZ of the dorsal dentate gyrus (*p=0.014, Mann-Whitney test). **F`** and **G`** are details of the squared areas in **F** and **G**, respectively. Nuclear staining in blue with DAPI.

Images were obtained under the confocal microscope, and a Z-stack of 10 μm was composed with ImageJ software in **B, C, F**, and **G**. 1-μm-thick pictures are shown in **F`**, and **G`**.

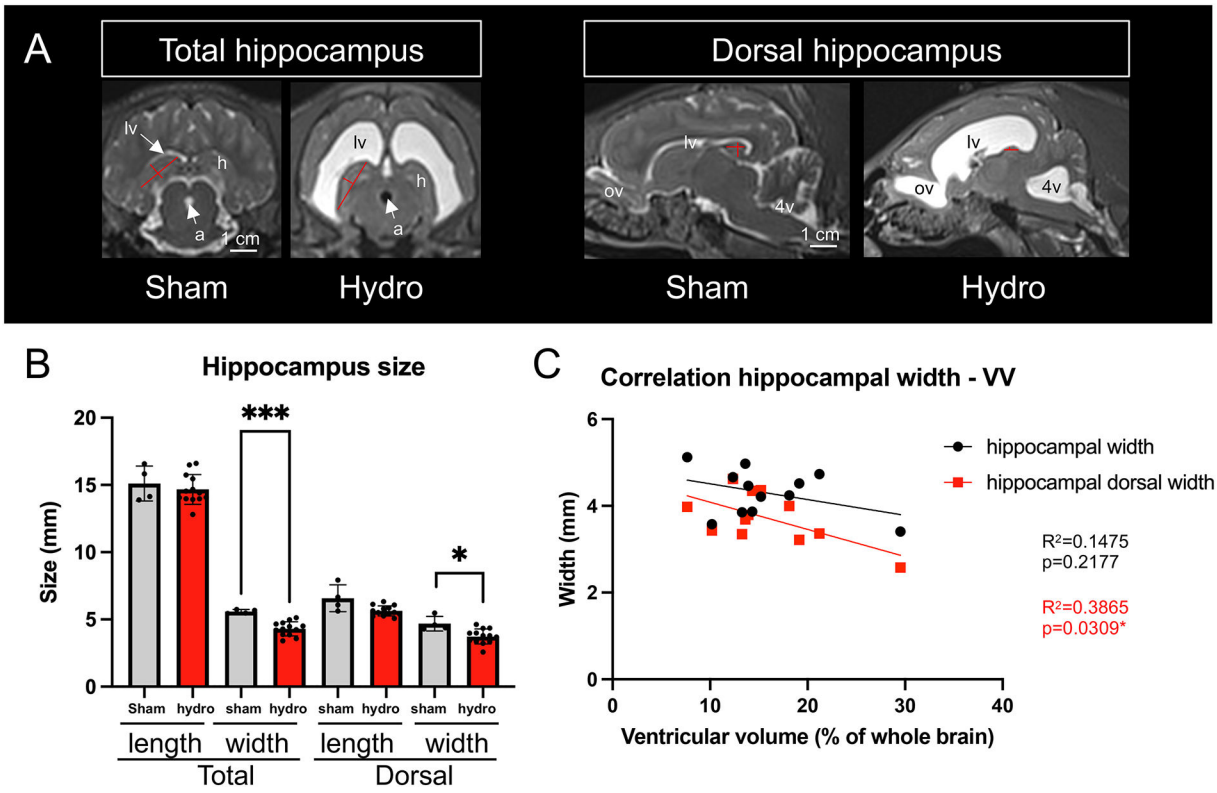

FIGURE 5. Hippocampal size and correlation with ventricular volume at 14 ± 4 days post-induction.

(**A, B**) Widths of the entire hippocampus and the dorsal hippocampus were significantly reduced in hydrocephalic pigs compared to sham control pigs (***p=0.0008 and *p=0.0151, respectively, Mann-Whitney test) in contrast to the hippocampal length. Length and width were measured as shown in **A** (red lines). Scale bar is identical for all panels. Coronal views are shown for total hippocampus and sagittal views for dorsal hippocampus. (**C**) In addition, the dorsal hippocampal width did correlate with the increase in ventricular volume (R^2=0.3865, p=0.0309*, Simple linear regression, *red*) in hydrocephalic pigs. Ventricular volume was normalized by total brain volume. Two sham controls and eight hydrocephalic pigs were excluded from this analysis because of the unavailability of MRI and/or cognitive testing. Abbreviations: a, aqueduct; h, hippocampus; lv, lateral ventricle; ov, olfactory ventricle; 4v, fourth ventricle.

Table 1.

Primary antibodies.

Antibody	Target	Manufacturer	Catalogue number	Research Resource Identifier (RRID)	Dilution	Host
DCX	Neuronal progenitor cells	Abcam	Ab18723	AB_732011	1:500	Rabbit
Iba1	Microglia	Wako (Fisher Scientific)	NC9288364	AB_839504	1:500	Rabbit
NeuN	Neurons	Millipore	Abn78	AB_10807945	1:100	Rabbit
Vimentin	Reactive astrocytes	Abcam	Ab92547	AB_10562134	1:200	Rabbit

Table 2.

Exploratory behavior of pigs during the test trial of the novel object recognition (NOR) task; comparison of pre induction and post induction time-points in hydrocephalic pigs.

Behavioral Measures	Time-point		Pooled SEM[1]	*p*-value[2]
	Pre induction	Post induction		
Recognition Index	0.598†	0.586†	0.039	0.822
Exploration of the *novel* object				
Object visit time, s	47.75	86.57	10.79	***0.009**
Number of object visits	8.3	7.2	0.87	0.353
Mean object visit time, s	6.57	13.59	1.88	***0.007**
Latency to first object visit, s	24.39	33.3	7.99	0.407
Latency to last object visit, s	248.45	242.7	11.18	0.701
Exploration of the *sample* object				
Object visit time, s	28.8	52.36	6.46	***0.009**
Number of object visits	6.8	6.4	0.5	0.560
Mean object visit time, s/visit	4.29	9.36	1.37	***0.007**
Latency to first object visit, s	27.93	32.77	9.78	0.712
Latency to last object visit, s	240.92	235.69	11.97	0.745
Exploration of *both* objects				
Total object visit time, s	76.56	138.92	13.96	***0.002**
Number of object visits	15.1	13.6	1.06	0.297
Mean object visit time, s/visit	5.29	11.23	1.33	***0.002**
Latency to first object visit, s	7.3	9.46	3.4	0.635
Latency to last object visit, s	272.82	267.65	6.17	0.532

†Recognition index value is different ($P < 0.05$) from that of chance (0.50).

[1]Abbreviation: SEM, standard error of mean.

[2]*P*-value for the overall 1-way ANOVA, which included a single fixed effect of time-point.